MINERALOGICAL MAGAZINE, DECEMBER 1971, VOL. 38, PP. 471–80

The join $CaMgSi_2O_6$–$Ca_2MgSi_2O_7$–$CaTiAl_2O_6$ in the system CaO–MgO–Al_2O_3–TiO_2–SiO_2 and its bearing on titanpyroxenes

KOSUKE ONUMA *and* KENZO YAGI
Department of Geology and Mineralogy, Hokkaido University, Sapporo, Japan

SUMMARY. The phase equilibrium diagrams of $CaMgSi_2O_6$–$CaTiAl_2O_6$ with 10, 20, and 30 wt % $Ca_2MgSi_2O_7$ in the join $CaMgSi_2O_6$–$Ca_2MgSi_2O_7$–$CaTiAl_2O_6$ were determined. Six three-phase assemblages, six four-phase assemblages, and two five-phase assemblages (isobaric trivariant, divariant, and univariant) were confirmed. The univariant assemblages are diopside$_{ss}$+forsterite+åkermanite$_{ss}$+perovskite+liquid and diopside$_{ss}$+åkermanite$_{ss}$+perovskite+spinel+liquid.[1] Because of the complex solid solutions of diopside and åkermanite the crystallization ceases before invariant assemblages are reached and the final phase assemblage in the diopside-rich region is diopside$_{ss}$+åkermanite$_{ss}$+perovskite, in the diopside-poor region diopside$_{ss}$+åkermanite$_{ss}$+perovskite+spinel. Two invariant points, diopside$_{ss}$+forsterite+åkermanite$_{ss}$+perovskite+spinel+liquid and diopside$_{ss}$+åkermanite$_{ss}$+anorthite+perovskite+spinel+liquid in the silica-poor region of the system CaO–MgO–Al_2O_3–TiO_2–SiO_2 are estimated. The diopside solid solution in this join is discussed with its bearing on the natural titanpyroxenes from alkalic rocks including melilite.

THE system $CaMgSi_2O_6$–$Ca_2MgSi_2O_7$–$CaTiAl_2O_6$ is a part of the system $CaMgSi_2O_6$–$Ca_2MgSi_2O_7$–$NaAlSiO_4$–$CaTiAl_2O_6$ and a join in the quinary system CaO–MgO–Al_2O_3–TiO_2–SiO_2. In our previous paper (Yagi and Onuma, 1969) the data for liquidus, some subsolidus, and solidus temperature regions of the present join were presented. However, more complete data for subsolidus and solidus temperatures are given in the present paper together with descriptions of phase relations.

Osborn and Gee (1969) have presented the liquidus data for the 15 wt. % Al_2O_3+TiO_2 plane in the system CaO–MgO–Al_2O_3–TiO_2–SiO_2; this study was made to contribute primarily to an understanding of the role of titanium from a ceramic rather than a petrologic viewpoint. In the present paper we have discussed the phase relation between diopside, åkermanite, perovskite, and spinel, which are encountered in the present join, with emphasis on the mineralogical and petrological aspect of the equilibrium in the silicate systems.

Experimental results. In the present investigation ordinary quenching methods were employed. The starting material was prepared by complete crystallization of homogeneous glass at temperatures between 800 °C and 1000 °C. The furnace used in quenching experiments was regulated to a precision of ±1 °C. Pt–$Pt_{87}Rh_{13}$ thermocouples used to measure the temperature were calibrated at the standard melting points of NaCl, 800·4 °C, Au, 1062·6 °C, and diopside, 1391·5 °C (the Geophysical

[1] ss = solid solution.

Laboratory temperature scale was used for consistency with our previous data). The duration of runs was 2 to 3 hours at temperatures above 1250 °C, 5 to 6 hours around 1240 °C, 2 to 4 days around 1230 °C, and 7 to 14 days at temperatures for beginning of melting.

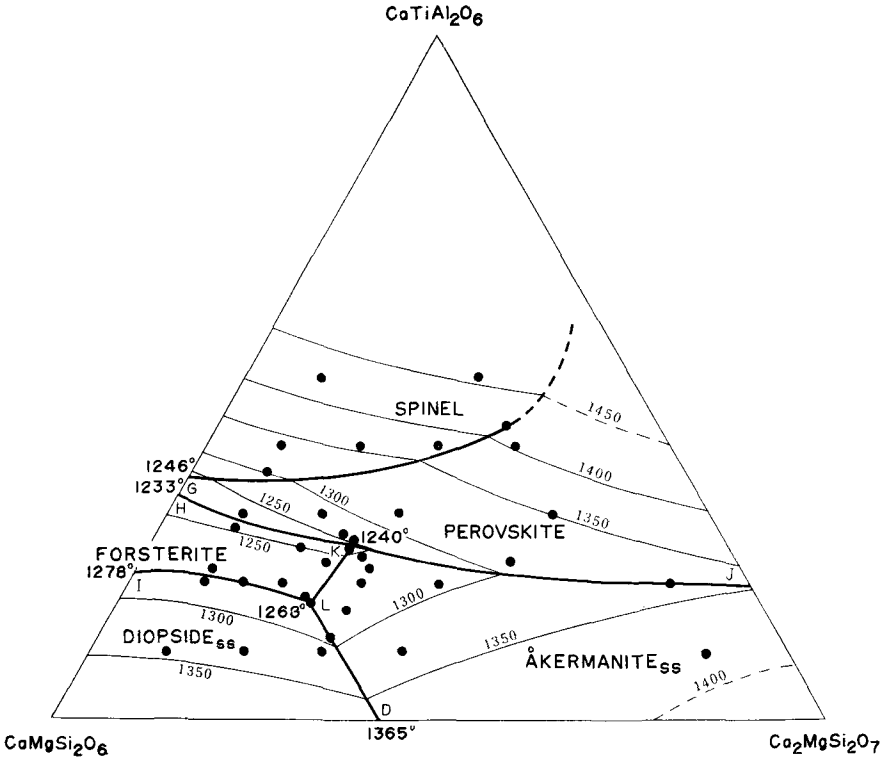

FIG. 1. Phase equilibrium diagram of the join $CaMgSi_2O_6$–$Ca_2MgSi_2O_7$–$CaTiAl_2O_6$ at liquidus. ss = solid solution.

Diopside (Di), åkermanite (Åk), forsterite (Fo), spinel (Sp), and perovskite (Pv) are the crystalline phases encountered in the present join and the first two are not pure compounds but solid solutions. The phase equilibrium diagram at the liquidus temperature is given in fig. 1. Because of the quinary nature of the join the points K and L in fig. 1, showing four-phase assemblages Pv+Fo+$Åk_{ss}$ (ss: solid solution)+L (liquid) (K) at 1240 °C and Di_{ss}+Fo+$Åk_{ss}$+L (L) at 1268 °C, are neither eutectic nor piercing points.

Sections with 10, 20, and 30 wt. % $Ca_2MgSi_2O_7$ (Åk) were studied (figs. 2, 3, and 4; table I). Each section exhibits a closed field of forsterite crystallization, which demonstrates a forsterite–liquid reaction. In these compositions this leads to the complete resorption of forsterite prior to solidification. Thus forsterite is resorbed in the equilibria: Fo+Di_{ss}+L; Fo+Di_{ss}+Pv+L; Fo+Di_{ss}+$Åk_{ss}$+L; and Fo+Di_{ss}+$Åk_{ss}$+Pv+L.

TABLE I. *Result of quenching experiments.*

Composition (wt. %)			Primary phase	Liquidus temp. (° C)	Data at lower temperatures
Di	Åk	Tp			
80	10	10	Di	1330	Åk in 1268, Pv in 1222, B.M. 1185
70	10	20	Di	1273	Åk in 1238, Pv in 1238, B.M. 1190
68	10	22	Fo	1265	Di in 1263, Fo out 1240, Pv in 1233, Åk in 1230
62	10	28	Fo	1265	Pv in 1256, Di in 1230, Fo out 1224, Åk in 1223
60	10	30	Pv	1250	Di in 1229, Åk in 1215, B.M. 1210.
54	10	36	Sp	1300	Pv in 1281, Di in 1235, Åk in 1228
50	10	40	Sp	1347	Pv in 1330, Di in 1229, B.M. 1210
40	10	50	Sp	1443	Pv in 1373, Di in 1234
70	20	10	Di	1321	Åk in 1250, Pv in 1227, B.M. 1180
60	20	20	Fo	1261	Di in 1249, Pv+Åk in 1233, Fo out 1242, B.M. 1185
55	20	25	Fo	1255	Di in 1239, Pv in 1233, Fo out 1234, Åk in 1232
50	20	30	Pv	1250	Di in 1236, Åk in 1233
40	20	40	Sp	1265	Pv in 1348, Di in 1228, Åk in 1223
60	30	10	Di	1308	Åk in 1306, Pv in 1230
58	30	12	Di+Åk	1301	Fo in 1280, Fo out 1275, Pv in 1234
54	30	16	Åk	1285	Fo in 1273, Di in 1268, Fo out 1235, Pv in 1233
50	30	20	Åk	1275	Fo in 1262, Di in 1249, Fo out 1231, Pv in 1228
48	30	22	Åk	1268	Fo in 1255, Di in 1234, Pv in 1232, Fo out 1225
40	30	30	Pv	1307	Åk in 1248, Fo in 1231, Di in 1229, Fo out 1225
30	30	40	Sp	1386	Pv in 1378, Åk in 1280 Di in 1223, B.M. 1190
20	30	50	Sp	1450	Pv in 1445, Åk in > 1300, Di in 1225, B.M. 1195

Åk: åkermanite; Di: diopside; Fo: forsterite; Pv: perovskite; Sp: spinel; Tp, $CaTiAl_2O_6$; B.M.: beginning of melting.

The maximum temperatures at which the assemblages $Di_{ss}+Åk_{ss}+Fo+Pv+L$ and $Di_{ss}+Åk_{ss}+Sp+Pv+L$ were encountered as piercing points are 1234 ± 5 °C and 1224 ± 5 °C, respectively.

As a result of the extensive solid solution in diopside and in åkermanite, crystallization ceases before any six-phase assemblage (invariant assemblage) is encountered.

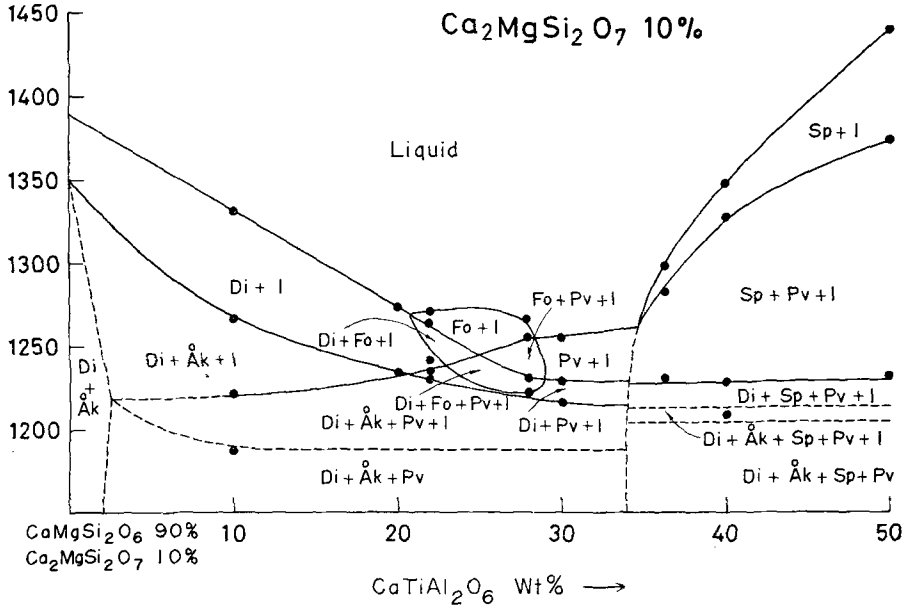

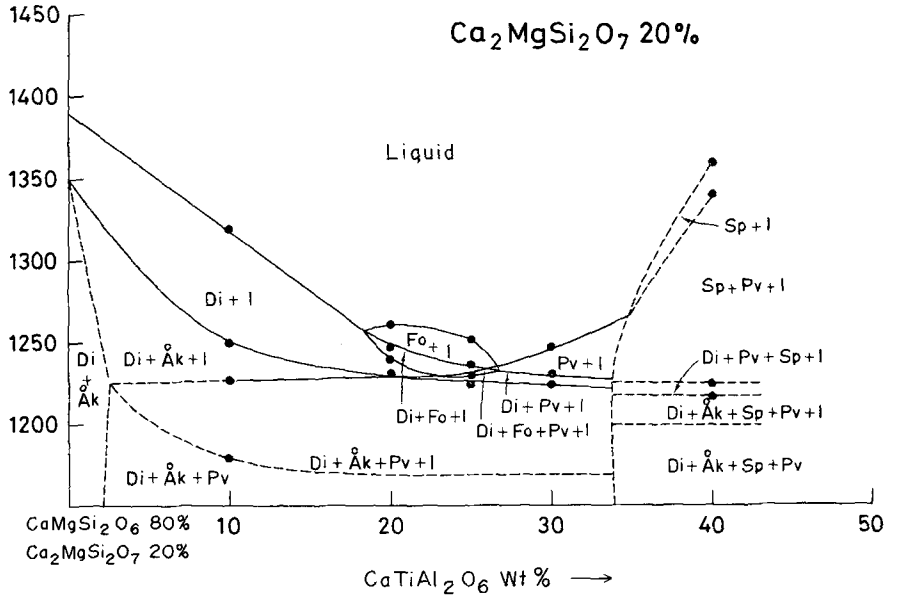

FIGS. 2 (top) and 3 (bottom). Phase equilibrium diagrams of 10 and 20 wt % $Ca_2MgSi_2O_7$ sections in the join $CaMgSi_2O_6$–$Ca_2MgSi_2O_7$–$CaTiAl_2O_6$. Åk, åkermanite solid solution; Di, diopside solid solution; Fo, forsterite; Pv, perovskite; Sp, spinel.

In the diopside-rich region crystallization ceases in the equilibrium $Di_{ss}+Åk_{ss}+Pv+L$ and elsewhere in the equilibrium $Di_{ss}+Åk_{ss}+Sp+Pv+L$, which was encountered from 1224±5 °C down to 1205±5 °C in the 10 % section, 1200±5 °C in the 20 % section, and 1195±5 °C in the 30 % section.

The composition of the åkermanite solid solution that crystallizes at 1000 °C in 7 to 14 days in the 30 % section was assessed from its d_{211} spacing (fig. 5). The åkermanite solid solution is constant in the three-phase assemblage $Di_{ss}+Åk_{ss}+Pv$

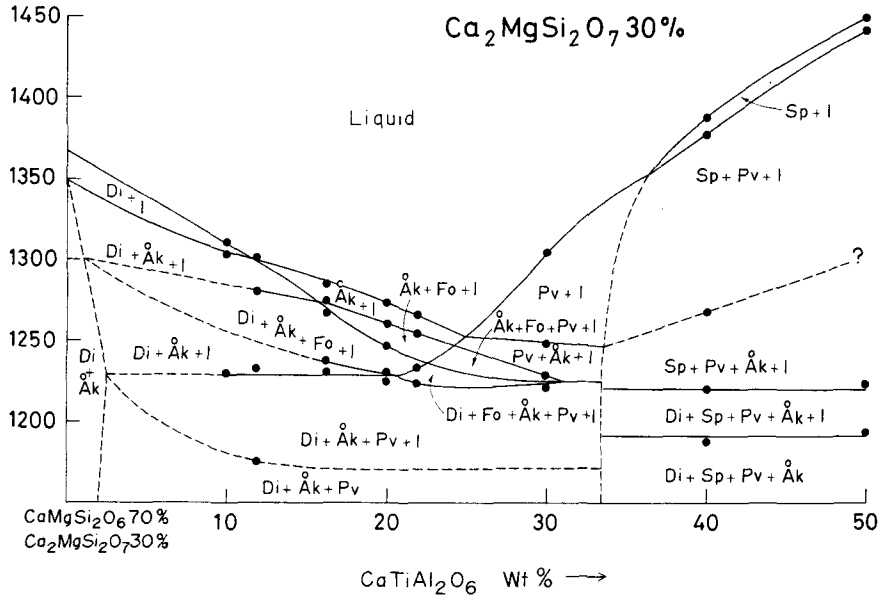

FIG. 4. Phase equilibrium diagram of 30 wt % $Ca_2MgSi_2O_7$ section.

indicating that as $CaTiAl_2O_6$ increases, only the diopside solid solution changes. At higher $CaTiAl_2O_6$ contents spinel appears and at the same time the åkermanite solid solution becomes more aluminous (gehlenite-rich).

Suggested flow diagram for parts of the system CaO–MgO–Al_2O_3–TiO_2–SiO_2. A suggested flow diagram (fig. 6) shows six-phase assemblages (invariant) in pentagonal boxes (liquid is omitted from all asemblages) and five-phase assemblages (univariant) as lines. The five-phase assemblages shown by the heavy lines were encountered in the sections studied over the temperature ranges reported above and repeated in fig. 6. None of the inferred six-phase assemblages has been experimentally encountered. However, combining these two five-phase lines and those estimated from O'Hara and Biggar's study (1969) ($Di_{ss}+Fo+Åk_{ss}+Sp+L$ and $Di_{ss}+An+Åk_{ss}+Sp+L$), two six-phase assemblages are produced (A and B in fig. 6).

The four-phase assemblages are diagramatically represented as light lines, which form crosses on the five-phase lines and are elaborated in the lower part of fig. 6.

The dot-dashed line represents an equilibrium crystallization path in which forsterite is resorbed and åkermanite solid solution appears in the åkermanite-poor region (10 and 20 % sections). After forsterite is resorbed the crystallization trend leaves the four-phase line (Di_{ss}+Fo+Pv+L) to follow the dot-dashed line (Di_{ss}+Pv+L), where diopside solid solution changes its composition and perovskite continues to crystallize until another four-phase line (Di_{ss}+$Åk_{ss}$+Pv+L) is reached.

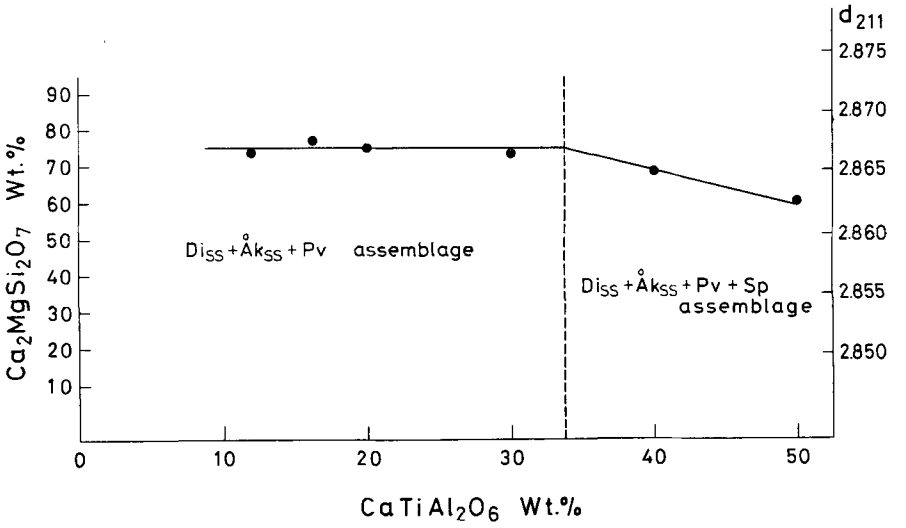

FIG. 5. Change of 211 *d*-spacing and composition of the åkermanite solid solution crystallized at 1000 °C for 7 to 14 days in the 30 wt % $Ca_2MgSi_2O_7$ section.

In the åkermanite-rich region (30 % section) the crystallization on the four-phase lines of both Di_{ss}+$Åk_{ss}$+Fo+L and Fo+$Åk_{ss}$+Pv+L reaches the five-phase line Di_{ss}+$Åk_{ss}$+Fo+Pv+L at various temperatures between 1225 °C and 1234 °C, where forsterite begins to react with liquid. When forsterite disappears along this five-phase line, the crystallization turns its course to the four-phase line Di_{ss}+$Åk_{ss}$+Pv+L.

Crystallization on the remaining four-phase lines, which do not include the forsterite–liquid reaction, is simple and needs no special description.

The pyroxenes in the join and in natural rocks. X-ray diffraction patterns of the diopside crystallized at 1000 °C for 7 to 14 days are shown in fig. 7. It is evident that the 002 peak shifts to lower angles and $\Delta 2\theta_{22\bar{1}-002}$ becomes larger with increasing $CaTiAl_2O_6$ in the mixture from which diopside solid solution crystallizes out.

In the diopside-rich region the three-phase assemblage Di_{ss}+$Åk_{ss}$+Pv was encountered at the solidus temperature and the following reaction is expected:

$$\underset{\text{diopside}}{CaMgSi_2O_6}+\underset{\text{åkermanite}}{Ca_2MgSi_2O_7}+2CaTiAl_2O_6 = \underset{\text{enstatite}}{2MgSiO_3}+\underset{\text{Tchermak's molecule}}{CaAl_2SiO_6}+\underset{\text{gehlenite}}{Ca_2Al_2SiO_7}+\underset{\text{perovskite}}{2CaTiO_3}$$

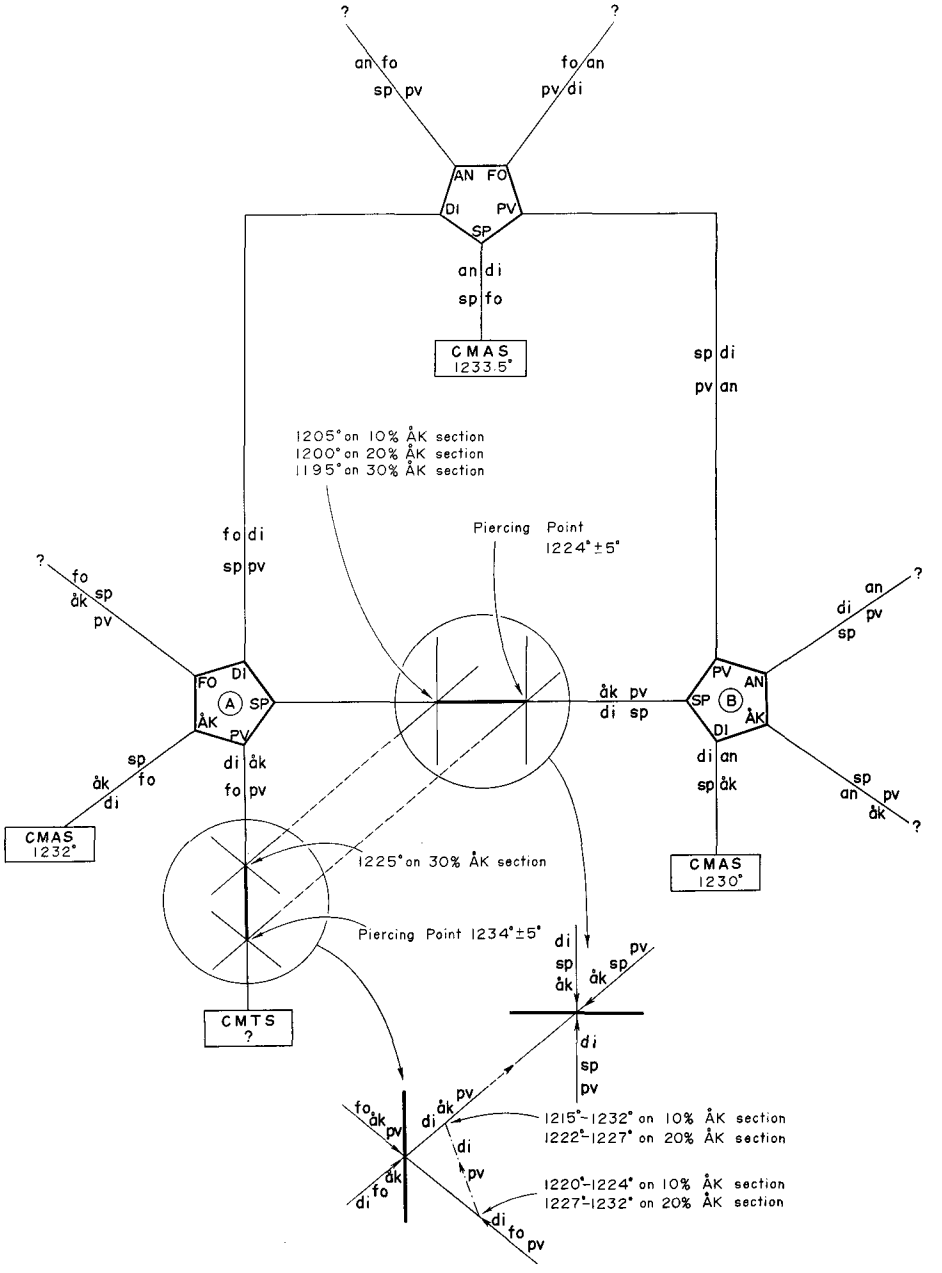

FIG. 6. Suggested flow diagram for parts of the system CaO–MgO–Al_2O_3–TiO_2–SiO_2, showing confirmed and possible phase assemblages. Explanations are given in text. CMAS, system CaO–MgO–Al_2O_3–SiO_2; CMTS, system CaO–MgO–TiO_2–SiO_2; åk, åkermanite (solid solution); an, anorthite; di, diopside (solid solution); fo, forsterite; pv, perovskite; sp, spinel. Arrows in the lower part of the figure show crystallization trends.

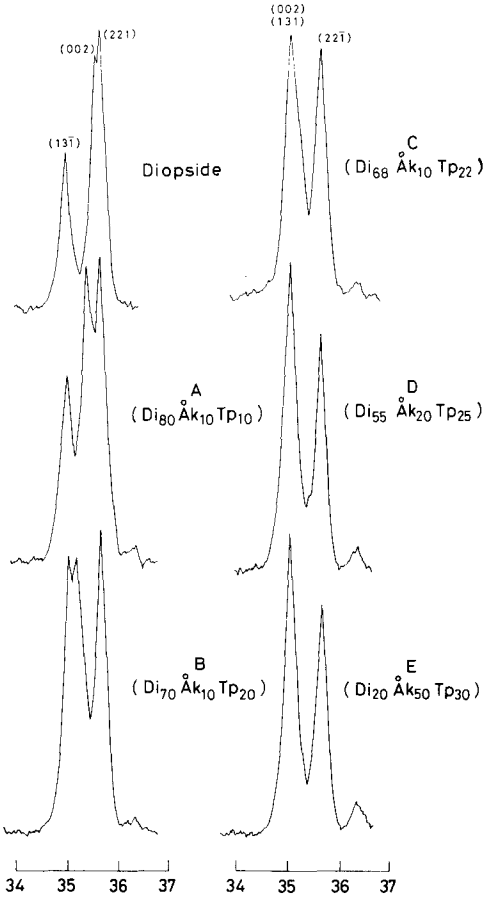

FIG. 7. X-ray diffraction patterns of diopside solid solutions crystallized at 1000 °C for 7 to 14 days, showing the shift of the 002 peak. Tp: $CaTiAl_2O_6$.

TABLE II. *Molecular composition of titanpyroxenes*

	1	2	3	4
$Ca(Mg,Fe)Si_2O_6$	69·5	66·5	73·4	88·4
$(Mg,Fe)SiO_3$	5·0	1·5	2·1	2·3
$Ca(Al,Fe^{3+})_2SiO_6$	12·7	19·0	10·2	
$CaTi(Al,Fe^{3+})_2O_6$	8·7	11·7	10·7	5·7
$NaFe^{3+}Si_2O_6$	4·6	2·8	5·1	2·7*
SiO_2	−0·8	−1·8	−0·5	1·5

* Including Na_2SiO_3 0·9 wt %.

1. Titanclinopyroxene, kalsilite-bearing olivine melilitite, Nyiragongo, Africa (Sahama and Meyer, 1958).
2. Titanaugite, melilite nepheline dolerite, Scawt Hill, Co. Antrim (Tilley and Harwood, 1931).
3. Titanclinopyroxene, melilite leucite nephelinite, Nyiragongo, Africa (Sahama and Meyer, 1958).
4. Groundmass pyroxene, melilitite, Nyiragongo, Africa (Sahama 1962).

On the other hand, the four-phase assemblage $Di_{ss}+Åk_{ss}+Sp+Pv$ was obtained at the solidus temperature in the diopside-poor region. This assemblage is expected from the reaction:

$$\underset{\text{diopside}}{CaMgSi_2O_6}+2\underset{\text{åkermanite}}{Ca_2MgSi_2O_7}+5CaTiAl_2O_6$$
$$= \underset{\substack{\text{Tchermak's}\\ \text{molecule}}}{3CaAl_2SiO_6}+\underset{\text{enstatite}}{2MgSiO_3}+\underset{\text{gehlenite}}{Ca_2Al_2SiO_7}+\underset{\text{perovskite}}{5CaTiO_3}+\underset{\text{spinel}}{MgAl_2O_4}$$

The diopside solid solution in the join, therefore, is assumed to consist of $CaMgSi_2O_6$, $CaAl_2SiO_6$, $CaTiAl_2O_6$, and $MgSiO_3$. Of these $CaTiAl_2O_6$ is found to be incorporated in the diopside solid solution up to 11 wt % in the join $CaMgSi_2O_6$–$CaTiAl_2O_6$ (Yagi and Onuma, 1967), but the reactions show that it may be possible that in the quaternary join $CaMgSi_2O_6$–$CaTiAl_2O_6$–$CaAl_2SiO_6$–$MgSiO_3$ more $CaTiAl_2O_6$ is soluble than this limit after perovskite separates out.

The present join is closely related to the undersaturated mafic alkalic rocks, especially melilite-bearing rocks from the view point of mineral assemblages (Yagi and Onuma, 1969). Therefore, the constituent molecules of natural titaniferous pyroxenes in the melilite-bearing rocks from various localities were calculated in terms of these molecules. Since the natural pyroxenes, however, contain FeO and Fe_2O_3, $Ca(Mg,Fe^{2+})Si_2O_6$ (diopside), $(Mg,Fe^{2+})SiO_3$ (hypersthene), $Ca(Al,Fe^{3+})_2SiO_6$ (Tchermak's molecule), and $NaFe^{3+}Si_2O_6$ (acmite) are calculated instead of iron-free molecules. If Al_2O_3 is less than TiO_2, $CaTiFe^{3+}_2O_6$ is calculated to form $CaTi(Al, Fe^{3+})_2O_6$.

The results of this calculation (table II) clearly show that the titaniferous pyroxenes of melilite- and nepheline-bearing rocks consist mainly of diopside, hypersthene, $CaTi(Fe^{3+}, Al)_2O_6$, and Tschermak's molecule, $Ca(Fe^{3+}, Al)_2SiO_6$, and have very small amounts of Na_2O, though these rocks always include nepheline.

According to the possible differentiation course of the melilite- and nepheline-bearing rocks (Onuma and Yagi, 1967), olivine melilitite → olivine melilite nephelinite → melilite nephelinite, the samples 1, 2 and 3, and 4 in table II may represent the pyroxenes at the early stage, middle stage, and later stage, respectively. So far as experimental data are concerned, if at the early stage melilite or forsterite or both crystallize, then as they include negligible amounts of titanium, the residual liquid becomes gradually rich in titanium and the pyroxene that is separated out from this liquid also becomes gradually rich in titanium. Thereafter the residual liquid begins to become poorer in titanium and furthermore, if perovskite begins to crystallize the decrease of titanium content in the liquid becomes more pronounced. In the natural magma titanium goes into not only perovskite but also into some oxide minerals such as ilmenite or magnetite. Consequently the pyroxenes crystallizing from such liquid at the later stage would be poorer in titanium.

Acknowledgement. Mr. S. Terada of Hokkaido University helped in the laboratory and in preparation of figures. Part of the cost for the present study was defrayed by a Grant for Scientific Research from the Ministry of Education of Japan, which is gratefully acknowledged.

REFERENCES

O'HARA (M. J.) and BIGGAR (G. M.), 1969. *Amer. Journ. Sci.* **267–A,** 364.
ONUMA (K.) and YAGI (K.), 1967. *Amer. Min.* **52,** 227.
OSBORN (E. F.) and GEE (K. H.), 1969. *Bull. Earth and Mineral Sci. Exp. Station, Pennsylvania State Univ.* no. 85, 57.
SAHAMA (TH. G.), 1962. *Trans. Edinburgh Geol. Soc.* **19,** 1.
—— and MEYER (A.), 1958. *Exploration du Parc National Albert,* **2,** *Inst. Parcs Nat. Congo Belge,* pp. 85.
TILLEY (C. E.) and HARWOOD (H. F.), 1931. *Min. Mag.* **22,** 439.
YAGI (K.) and ONUMA (K.), 1967. *Hokkaido Univ. Fac. Sci. Journ.* ser 3, **13,** 463.
—— —— 1969. *Amer. Journ. Sci.* **267–A,** 509.

[*Manuscript received 12 October 1970*]